How do interactions control droplet size during nanoprecipitation?

Robert Botet, Kevin Roger

How do interactions control droplet size during nanoprecipitation?

Robert Botet[a,*], Kevin Roger[b,**]

[a] *Laboratoire de Physique des Solides, CNRS UMR8502, Université Paris-Sud, Université Paris-Saclay, 91405 Orsay,France*
[b] *Laboratoire de Génie Chimique, CNRS UMR 5503, Université de Toulouse, F-31030 Toulouse, France*

Keywords:
Nanoprecipitation
Droplet
Coalescence
Computational methods
Scaling-law
Dynamics
Monodispersity
Solvent-shifting
Ouzo effect

A B S T R A C T

Nanoprecipitation provides colloidal dispersions through successive recombination events between nanometric objects. In the present article, we explain why the nanoprecipitation pathways induced through solvent-shifting – the Ouzo effect –, are fascinating study-cases. Indeed, they allow to address the question of how the interactions between the colloidal particles control the dynamics of the process, thus the particle size distribution. Experimental monitoring of the precipitation dynamics demonstrates that the colloidal dispersion polydispersity decreases over time as the droplets coalesce. Monte Carlo simulations within the Smoluchowski framework agree quantitatively with these observations, and show how the interactions between the particles naturally force the system to become nearly monodisperse. The mechanistic understanding gained from the solvent-shifting experiments is also relevant to other nanoprecipitation processes.

1. Introduction

Segregation often prevails amongst molecules, which makes phase separation a general behavior for multi-component mixtures. However, certain non-equilibrium pathways may trap the system at an intermediate length-scale between molecular mixing and macroscopic phase separation: the colloidal domain.

Top–down pathways lead to the formation of colloids through successive divisions of macroscopic domains into smaller ones. The associated free energy cost dramatically increases with the amount of interfaces. Colloids with sub-micronic dimensions (1–100 nm) are thus difficult to obtain. On the contrary, bottom–up pathways start from homogeneous solutions, in which molecules are mixed at the molecular scale, and rely on a parameter change to trigger phase separation. Generally, the bottom–up pathway only ensures appearance of growing microstructures, while the formation of colloids requires a specific control of the growing process (*i.e.* a stopping mechanism). Otherwise, the microscopic objects will continue to combine until equilibrium macroscopic phase separation. A typical hindering mechanism operates through the build-up of repulsive barriers between colloids of a given length-scale, thus keeping the colloidal system in a metastable state [1].

Behind this well-documented mechanism lies an important issue: how to control colloidal system uniformity. Indeed, "monodisperse" dispersions, consisting of identical colloidal objects, are often desired as their physical properties are generally easier to control than those of "polydisperse" dispersions. Therefore, we want to understand how the interactions between colloids, and thus the barriers that oppose their recombinations, relate to the colloidal dispersion size distribution.

2. The Ouzo effect: nanoprecipitation through solvent-shifting

The addition of a bad solvent to a solute/good solvent mixture is an interesting study case of bottom–up pathways. Indeed, this solvent-shifting results in the spontaneous precipitation of the solute into a mixture of the two solvents, as observed routinely when preparing an anise-based beverage such as Ouzo. Furthermore, this process does not involve any chemical reactions, contrarily to most nanoprecipitation methods.

However, a complication arises from the mixing kinetics of the two solvents. Consider the system in its initial state: a solute is dissolved in one of its good solvents. Addition of a bad solvent that mixes with the good solvent decreases the overall solvent quality. The solute

* Correspondence to: Laboratoire de Physique des Solides, 1 rue Nicolas Appert Bâtiment 510 91405 Orsay, Cedex, France.
** Correspondence to: Laboratoire de Génie Chimique, 4 allée Emile Monso, 31432 Toulouse France.
E-mail addresses: robert.botet@u-psud.fr (R. Botet), kevin.roger@ensiacet.fr (K. Roger).

http://dx.doi.org/10.1016/j.cocis.2016.03.003

remains dissolved into a mixture of these two solvents, forming a single phase, up to a given amount of bad solvent, which corresponds, on a phase diagram, to reaching the solubilization boundary or binodal line. Upon crossing this phase boundary, the system starts to separate into two phases of distinct compositions given by the tie lines. However, the system has not reached its final composition yet and its representative point continues to move towards its final location, given by the global composition. A competition thus occurs between the splitting of the representative point into two sub-points along the tie line and the movement of the representative point towards its final location. This sums up as the following question: is mixing faster or slower than phase separation? Two cases can be considered, as illustrated on Fig. 1:

- if full mixing is achieved prior to phase separation, phase separation proceeds homogeneously in the sample. Interactions between the forming colloidal particles determine the final size distributions.
- if phase separation proceeds simultaneously with mixing, the system becomes heterogeneous. On a phase diagram, each mixing domain is associated with a different representative point and the effective trajectories may be complicated. Both the extent of this heterogeneity and its effect on the interactions between colloidal particles determine the final size distributions.

The latter is the most common situation in literature and has resulted in a number of observations, leading authors to distinguish between successful and unsuccessful solvent-shifting, separated by an "Ouzo-boundary". However, one should be careful since heterogeneities are hard to control and make conclusions unreliable. In particular, all the relevant parameters (concentration, solvent ratio, ionic strength) are changing in space and time while phase separation takes place. Most of the literature on nanoprecipitation through solvent-shifting belongs to this category [2•].

To overcome this difficulty, Prud'homme's group pioneered the use of efficient mixing cells to perform solvent-shifting in homogeneous conditions. The initial design used two confined impinging jets, adapted from Hartridge&Roughton mixers. Mixing times below a few milliseconds were achieved due to highly turbulent flows [3•]. However, this setup requires streams of equal momentum and thus realizes only a 1-1 mixing ratio. They therefore developed a multi-inlet vortex mixer with tangential streams that allows the mixing of streams of equal or non-equal momentum [4]. A large range of mixing ratios can then be used, which allows to explore the whole phase diagram.

Rapid mixing tools have also been used for decades in commercial instruments such as stopped-flow devices. However, since the mixing chambers have been designed mainly for aqueous solutions mixing, their applicability or solvent-shifting is problematic. Nevertheless, Roger et al. [5••] used a commercial stopped-flow from BioLogic company coupled to the intense X-ray beam of the ESRF synchrotron facility (instrument ID02). The first measurement was performed 10 ms after mixing and regular monitoring showed that colloidal dispersion reaches its metastable size distribution in about a second. This demonstrates that practical uncoupling of mixing (a few milliseconds) and phase separation (one second) is possible using adequate mixers.

3. The repulsive barriers

In the case where all components are liquid, the bottom–up solvent-shifting process occurs through a sequence of droplet coalescence. Droplet surfaces are generally electrically charged [6, 7], and the interaction between two droplets is the sum of a long-range attractive potential (Van der Waals attraction) and a small-range repulsive potential (double-layer electrostatic repulsion). This is the basis of the DLVO theory [1, 8, 9].

For two charged spheres of radius R_i and R_j respectively, with h being the distance between their two surfaces, the total interaction energy writes:

$$U_{ij} = \frac{R_i R_j}{R_i + R_j}\left(-\frac{A_H}{6}\frac{1}{h} + \Gamma e^{-\kappa h}\right) \quad (1)$$

A_H is the Hamaker constant for the liquid forming the droplets (A_H is a few k_BT) and quantifies the Van der Waals attraction. Γ quantifies the repulsion between two ionic double-layers and can be expressed either using effective surface charge densities [10] or effective electric potentials [11]. It is independent of the values of the radii at

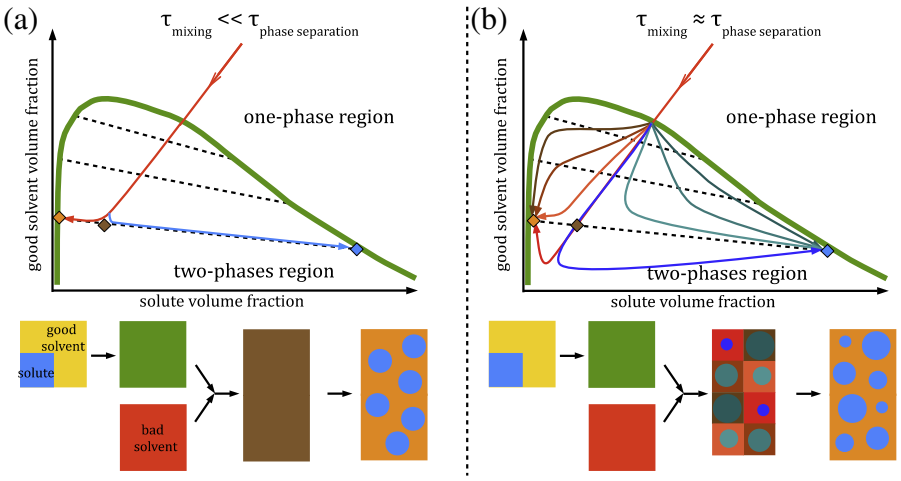

Fig. 1. Typical phase diagram for a solute (blue)/good solvent (yellow)/bad solvent (red) ternary system. The addition of a bad solvent leads to a phase separation upon crossing the solubilization boundary (green line). The compositions of each separating phase are given by the tie lines (dotted lines). (a) Corresponds to uncoupled mixing and phase separation. Rapid mixing brings the system to a homogeneous supersaturated solution at the final composition, which then phase separates. (b) Corresponds to simultaneous mixing and phase separation. Phase separation occurs at different and varying compositions. These heterogeneous conditions usually lead to less uniform dispersions.

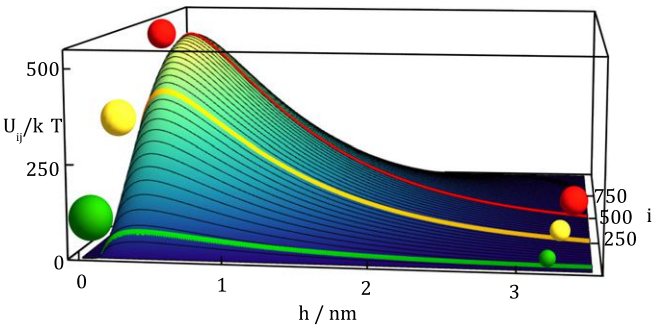

Fig. 2. Sketch of the interaction energy profile between two charged spherical particles. The sum of the radii is 1000 nm. The other parameters entering the relation (1) are: $A_H = 3k_BT$, $\Gamma = 4k_BT$/nm and the screening Debye length is $\kappa^{-1} = 1$ nm. The interaction energy, $U_{i,j}$, counted in k_BT unit, is plotted as a function of h (the separation between both surfaces) and R_i, the radius of the droplet labeled i. The other droplet radius is $R_j = (1000 - R_i)$ with R_i and R_j in nm. Three curves are highlighted: in green, the energy profile for the radii 25 nm and 975 nm; in yellow, the energy profile for the radii 250 nm and 750 nm; in red, the energy profile for the case $R_i = R_j = 500$ nm. The repulsive barrier is much lower – hence coalescence favored – when values of the radii are very different.

the leading order. κ^{-1} is the Debye screening length (typically a few nanometers). The relation (1) supposes that the radii are much smaller than the Debye length and that the separation h is smaller than the sum of the radii, $R_i + R_j$.

If the ionic repulsion dominates over the Van der Waals attraction, two droplets are hindered to come into contact by a repulsive barrier. Coalescence efficiency is then controlled by the height of this barrier. Fig. 2 displays the shape of the interaction free energy between two droplets labeled i and j, of respective radius R_i and R_j, with constant sum $R_i + R_j = 1000$ nm.

In a more precise way, the probability per unit of time of coalescence of two droplets is the product of the probability of collision (which depends on the diffusion, either free Brownian or induced by hydrodynamic) and of the probability that the colliding droplets pass over the repulsive barrier. The latter probability is generally defined as the inverse of the stability ratio [12], $W_{i,j}$. The larger the stability ratio, the smaller is the probability to coalesce. This ratio was studied in detail in the framework of the DLVO theory by Reerink and Overbeek [13]. They proved that $W_{i,j}$ is essentially equal to the exponential of the maximum of the interaction energy, $U_{\max}/k_BT$, which is typical of activated processes. Knowing the relation (1), one obtains:

$$W_{i,j} \propto \exp\left(\frac{\Gamma}{k_BT}\frac{R_iR_j}{R_i+R_j}\right). \tag{2}$$

A precise calculation gives the proportionality factor in Eq. (2), which is only weakly varying with the radius, whatever the transport process.

From the height of the barrier given by Eq. (2) and illustrated in Fig. 2, we can qualitatively predict how the system will evolve over time, and specify the corresponding mechanism. Indeed, for nearly equal-sized droplets (red curve on Fig. 2) – which corresponds to the middle of the size distribution –, highly repulsive barriers (height$\gg k_BT$) lead to very large stability factor, and coalescence is thus strongly hindered. At the same time, very different-sized droplets – which correspond to the tails of the size distribution –, experience relatively small repulsive barriers (height$\sim k_BT$) to overcome (green curve on Fig. 2) and coalescence proceeds more readily. Therefore the droplets in the tails of the size distributions coalesce much faster than the droplets in the middle of the size distribution, and the system evolves naturally towards the monodisperse state. In practice, in order to observe this selection rule, the stability ratio must be large enough for the hindrance mechanism to develop, but not that large that the kinetics be inaccessible. We will now discuss quantitative approaches.

4. The coalescence equations

A century ago, Smoluchowski [14] wrote the kinetic rate equations, which describe the number of droplets over time, as a difference between a gain term and a loss term, which are both due to coalescence events. The experimental conditions are gathered in the coalescence kernel function, $K_{i,j}$, which is the probability of coalescence between a droplet labeled i and a droplet labeled j. After the discussion in the previous section, one knows that the coalescence kernel function is essentially equal to the inverse of the stability factor, $W_{i,j}$, which is given in Eq. (2).

Let us take the usual case where the droplets are labeled with their volume, that is: i denotes the volume of the droplet labeled i. The set of rate equations writes in terms of the concentrations of the droplets of volume k, $c_k(t)$:

$$\frac{dc_k}{dt} = \text{Gain Term} - \text{Loss Term} \tag{3}$$

$$\text{Gain Term} = \frac{1}{2}\sum_{i+j=k} K_{i,j}c_ic_j \tag{4}$$

$$\text{Loss Term} = \sum_i K_{i,k}c_ic_k \tag{5}$$

in which Eq. (4) is the rate of creation of droplets of volume k by coalescence of a droplet of volume i and a droplet of volume $j = k-i$, and Eq. (5) is the rate of disappearance of droplets of volume k by coalescence of these droplets with any other droplet. Eqs. (3)– (5) suppose that the total volume of the droplets is conserved.

In spite of strong assumptions to write the rate equations above – e.g. fluctuations of the spatial distribution of the droplets are neglected [15•] –, this analytic approach is known to be successful to explain and quantitatively describe the evolution of the dispersed system in most coalescence experiments.

4.1. The self-preserving solution

In appearance, the Smoluchowski equations appear easy to write, but finding the exact solution of this set of infinite number of coupled nonlinear equations is a formidable task, which has been solved in only a few simple cases.

In the case of rapid coalescence (that is: with a stability ratio of order 1), the system tends to macroscopic phase separation. Since there is no characteristic droplet volume other than the actual average volume, $\langle k\rangle$, it is natural to assume that the volume distribution should depend only on the non-dimensional ratio $k/\langle k\rangle$ [16]. Putting then the concentrations c_k under the "self-preserving" form (the term was coined in [17•]):

$$c_k \propto f\left(\frac{k}{\langle k\rangle}\right) \tag{6}$$

with f a still unknown positive function, the Smoluchowski equations (3)-(5) write in much simpler forms, allowing to obtain definite information about the shape of the function f. This self-preserving regime is also termed the first-scaling law.

One can note that, defining the moments of the droplet volumes as: $\langle k^s\rangle = \sum_k k^s c_k / \sum_k c_k$, the scaling relation (6) implies that the radius polydispersity, δ, is a constant:

$$\delta^2 \equiv \frac{\langle R^2\rangle - \langle R\rangle^2}{\langle R\rangle^2} = \frac{\int_0^\infty u^{2/3}f(u)du}{\left(\int_0^\infty u^{/3}f(u)du\right)^2} - 1 \tag{7}$$

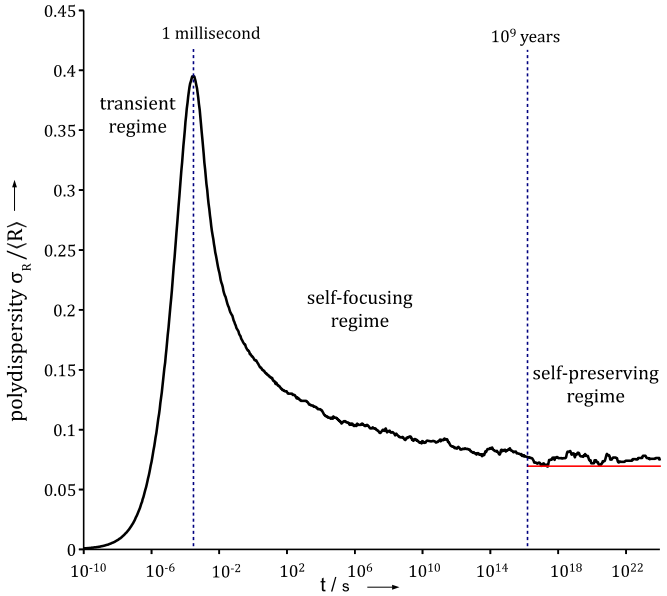

Fig. 3. Plot of the polydispersity, δ, as a function of elapsed time, for a system of spherical droplets coalescing with the Smoluchowski kernel (9). Monodisperse conditions are assumed, such that the initial value of the polydispersity is $\delta = 0$. After a burst in the polydispersity – reached in a few milliseconds –, the system tends to become more and more monodisperse over time. This self-focusing regime corresponds to a particular scaling termed the second-scaling. After a few billion years, the self-preserving regime is reached and the polydispersity reaches its predicted value.

since the droplet radius, R, is proportional to $k^{1/3}$ and $u{=}k/\langle k\rangle$ does not depend on time.

Strictly speaking, the self-preserving solution (6) is expected to be valid when the system is far from the initial state, that is when $\langle k\rangle \to \infty$ and $k/\langle k\rangle$ are finite. A common irritating problem in this approach, is the lack of information about the condition: $\langle k\rangle \to \infty$, hence the difficulty to know *a priori* whether an experimental system is in the scaling state (6) or not (transient behavior or alternative scaling).

4.2. Is the self-preserving scaling reached?

The case of the kinetic rate Eqs. (3)–(5) using the charged spheres kernel (that is essentially the inverse of the stability ratio Eq. (2)) was solved exactly in the self-preserving regime [18••]. A time-independent value of the polydispersity was obtained:

$$\delta \equiv \sqrt{\frac{\langle R^2\rangle - \langle R\rangle^2}{\langle R\rangle^2}} = 0.0664\ldots \tag{8}$$

However, one can wonder if the condition $t \to \infty$ is fulfilled in experiments, since the repulsive barrier likely implies large characteristic times.

To check this point, we performed numerical simulations of the Smoluchowski equations with the charged spheres kernel [5••]:

$$K_{i,j} = \frac{1}{\tau_{Br}}(R_i + R_j)^{\alpha}\left(\frac{1}{R_i} + \frac{1}{R_j}\right)^{\beta} e^{-\frac{\Gamma}{k_B T}\frac{R_i R_j}{R_i + R_j}} \tag{9}$$

in which α and β are characteristic exponents of the probability of collision of two Brownian spheres [17•], and τ_{Br} is a characteristic time for the Brownian coalescence of uncharged spheres.

On Fig. 3, numerical values of the polydispersity as a function of time are plotted for the charged spheres kernel (9), using typical experimental values as input, namely: $\Gamma = 1 k_B T/R_o$, with R_o the radius of the smallest sphere. The self-preserving regime is in fact reached, and the polydispersity reaches its predicted value Eq. (8), but only after an extremely long time of a few billion years. Therefore, in any experiments taking place under similar conditions, the exact self-preserving solution is irrelevant: another intermediate regime is present.

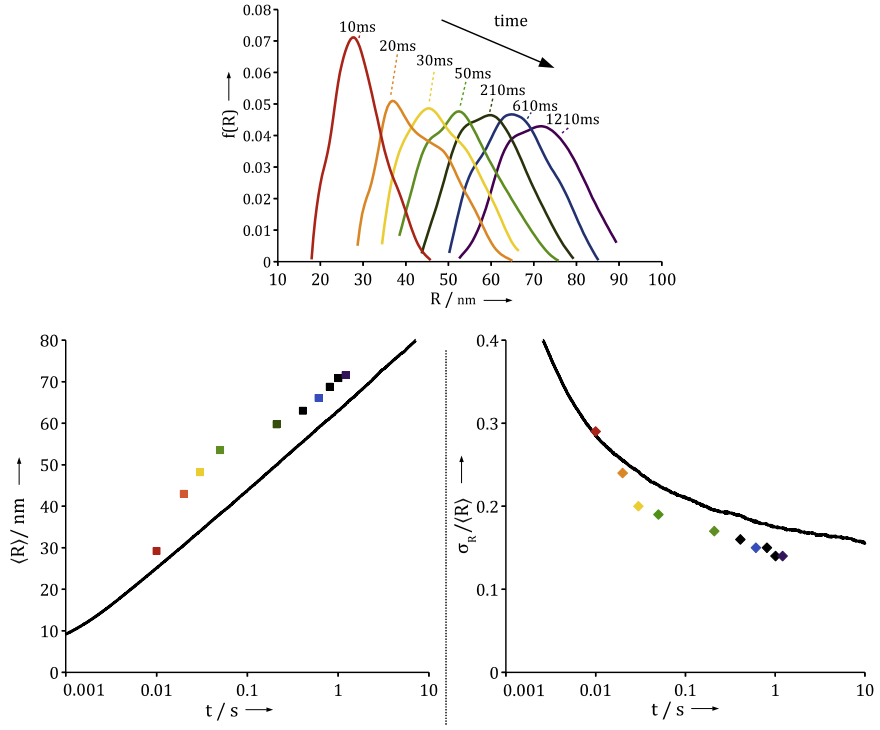

Fig. 4. Size distributions were obtained over time from SAXS experiments. The mean radius increases logarithmically over time, while the polydispersity decreases over time. Monte Carlo simulations using the charged kernel match the experimental variations, without any adjustable parameters.

Varying the Γ parameter in the numerical simulations, Roger, Botet and Cabane [5••] showed that this intermediate regime corresponds to a well-defined scaling of the size distribution, proper to small size fluctuations and different from Eq. (6). This second-scaling law corresponds to a characteristic temporal decrease: $\delta \propto 1/\sqrt{\langle R \rangle}$ [19].

4.3. The self-focusing scaling evidenced by experiments and simulations

The practical existence of this scaling law was investigated experimentally by Roger et al. on the model system PMMA/acetone/water [5••]. A rapid addition of water to the PMMA/acetone solution was ensured through the use of a stopped-flow device. Droplet growth was monitored through milliseconds-fast small-angle X-ray scattering at the ID02 beamline of the ESRF. The spectra were directly inverted using a method developed by Botet and Cabane based on the analysis of the deviation from the Porod law [20]. Size distributions were thus obtained without any assumptions about their shapes. These distributions and their first two moments, the mean radius and the polydispersity, are plotted on Fig. 4. A quantitative agreement with the simulation data was obtained without any adjustable parameters. The particles were charged through the macromolecules' end-groups [6] and the surface charge density was thus constant over time. This confirms that the self-focusing scaling is relevant in the practical case, while the self-preserving scaling is out of reach. This study also unveiled a mechanism through which successive recombination events lead to increasingly uniform colloidal dispersions.

5. Conclusion and perspectives

The combination of rapid mixers, numerical simulations and fast monitoring unveiled the mechanism responsible for obtaining narrow size distribution of colloidal dispersions prepared through solvent-shifting. The recombination dynamics of charged colloids fall into a characteristic scaling law under which the polydispersity decreases over time due to the size-dependent ionic repulsions. This mechanism should operate for a variety of other nanoprecipitation pathways and could explain why so many nanoparticle dispersions are uniform, even when the nucleation and growth mechanism has been shown not to operate [21]. However, a few experimental studies have demonstrated that narrow size distributions could also be obtained when the interfaces were nearly electrically neutral. Using block copolymers as stabilizers, Pinkerton et al. [22] prepared uniform dispersions of pharmaceutical drugs. This echoes with the limited-coalescence mechanism characterized by Whitesides et al. [23•] for particles stabilized emulsions. In both cases the stabilizing species adsorbs strongly to the interfaces, contrarily to short surfactants [24•, 25]. This suggests the existence of another self-focusing mechanism besides the one reviewed here, which applies to recombination between charged colloids.

6. Acknowledgment

We acknowledge Bernard Cabane for his essential collaboration on this topic.

References[•,••]

[1] Evans, F.D. Wennerström, H. The colloidal domain: where physics, chemistry, biology, and technology meet (advances in interfacial engineering), Wiley-VCH 1999, 0471242470. http://www.worldcat.org/isbn/0471242470.
[2•] Aubry, J. Ganachaud, F. Cohen Addad, J.-P. Cabane, B. Nanoprecipitation of polymethylmethacrylate by solvent shifting: 1. boundaries, Langmuir 25 (4) (2009) 1970–1979. http://pubs.acs.org/doi/pdf/10.1021/la803000e. http://pubs.acs.org/doi/abs/10.1021/la803000e. http://dx.doi.org/10.1021/la803000e.
[3•] Johnson, B.K. Prud'homme, R.K. Chemical processing and micromixing in confined impinging jets, AIChE J 49 (9) (2003) 2264–2282.
[4] Liu, Y. Cheng, C. Liu, Y. Prud'homme, R.K. Fox, R.O. Mixing in a multi-inlet vortex mixer (mivm) for flash nano-precipitation, Chem Eng Sci 63 (11) (2008) 2829–2842. http://www.sciencedirect.com/science/article/pii/S0009250907007774. http://dx.doi.org/10.1016/j.ces.2007.10.020.
[5••] Roger, K. Botet, R. Cabane, B. Coalescence of repelling colloidal droplets: a route to monodisperse populations, Langmuir 29 (19) (2013) 5689–5700. PMID: 23570451 http://dx.doi.org/10.1021/la400498j. http://dx.doi.org/10.1021/la400498j. http://dx.doi.org/10.1021/la400498j.
[6] Roger, K. Eissa, M. Elaissari, A. Cabane, B. Surface charge of polymer particles in water: The role of ionic end-groups, Langmuir 29 (36) (2013) 11244–11250. PMID: 23844840 http://dx.doi.org/10.1021/la4019053. http://dx.doi.org/10.1021/la4019053. http://dx.doi.org/10.1021/la4019053.
[7] Roger, K. Cabane, B. Why are hydrophobic/water interfaces negatively charged?, Angew Chem Int Ed 51 (23) (2012) 1521–3773.
[8] Derjaguin, B.L.L. Colloidal stability of protein-polymer systems: a possible explanation by hydration forces, Acta Physicochim USSR (1941).
[9] Verwey, E.J.W. Overbeek, J.T.G. Theory of the stability of lyophobic colloids, Elsevier, Amsterdam, 1948.
[10] Sader, J.E. Carnie, S.L. Chan, D.Y. Accurate analytic formulas for the double-layer interaction between spheres, J. Colloid Interface Sci 171 (1) (1995) 46–54. http://www.sciencedirect.com/science/article/pii/S0021979785711496. http://dx.doi.org/10.1006/jcis.1995.1149.
[11] Hogg, R. Healy, T.W. Fuerstenau, D.W. Mutual coagulation of colloidal dispersions, Trans Faraday Soc 62 (1966) 1638–1651. http://dx.doi.org/10.1039/TF9666201638. http://dx.doi.org/10.1039/TF9666201638.
[12] Fuchs, N. Zur theorie der koagulation, Z Phys Chemie A 171 (199-208) (1934).
[13] Reerink, H. Overbeek, J. The rate of coagulation as a measure of the stability of silver iodide sols, J Discuss Faraday Soc 18 (1954) 74–84.
[14] Smoluchowski, M. Drei vorträge über diffusion, brownsche molekularbewegung und koagulation von kolloidteilchen, Physik Zeit 17 (1916) 585–599.
[15•] Kang, K. Redner, S. Fluctuation effects in Smoluchowski reaction kinetics, Phys Rev A 30 (1984) 2833–2836. http://link.aps.org/doi/10.1103/PhysRevA.30.2833. http://dx.doi.org/10.1103/PhysRevA.30.2833.
[16] Friedlander, S. Theoretical considerations for the particle size spectrum of the sratospheric aerosols, J Meteor 29 (1961) 537–547.
[17•] Friedlander, S. Wang, C. The self-preserving particle size distribution for coagulation by brownian motion, J. Colloid Interface Sci 22 (1966) 126–132.
[18••] Dammer, S.M. Wolf, D.E. Self-focusing dynamics in monopolarly charged suspensions, Phys Rev Lett 93 (15) (2004) 150602.
[19] Botet, R. Ploszajczak, M. Universal fluctuations: the phenomenology of hadronic matter, World Scientific Publishing Co. Pte. Ltd, New Jersey, 2002.
[20] Botet, R. Cabane, B. Simple inversion formula for the small-angle X-ray scattering intensity from polydisperse systems of spheres, J Appl Crystallogr 45 (3) (2012) 406–416. http://dx.doi.org/10.1107/S0021889812012812. http://dx.doi.org/10.1107/S0021889812012812.
[21] Matijevic, E. Nanosize precursors as building blocks for monodispersed colloids, Colloid J 69 (1) (2007) 29–38.
[22] Pinkerton, N.M. Grandeury, A. Fisch, A. Brozio, J. Riebesehl, B.U. Prud'homme, R.K. Formation of stable nanocarriers by in situ ion pairing during block-copolymer-directed rapid precipitation, Mol Pharm 10 (1) (2013) 319–328. PMID: 23259920 http://dx.doi.org/10.1021/mp300452g. http://dx.doi.org/10.1021/mp300452g. http://dx.doi.org/10.1021/mp300452g.
[23•] Whitesides, T.H. Ross, D.S. Experimental and theoretical analysis of the limited coalescence process: stepwise limited coalescence, J Colloid Interface Sci 169 (1) (1995) 48–59. http://www.sciencedirect.com/science/article/pii/S0021979785710053. http://dx.doi.org/10.1006/jcis.1995.1005.
[24•] Lannibois, H. Hasmy, A. Botet, R. Chariol, O. Cabane, B. Surfactant limited aggregation of hydrophobic molecules in water, J Phys II 7 (2) (1997) 319–342. https://hal.archives-ouvertes.fr/jpa-00248446. http://dx.doi.org/10.1051/jp2:1997128.
[25] Lebouille, J. Stepanyan, R. Slot, J. Stuart, M.C. Tuinier, R. Nanoprecipitation of polymers in a bad solvent, Colloids Surf A Physicochem Eng Asp 460 (2014) 225–235. 27th European Colloid and Interface Society conference (27th {ECIS} 2013). http://www.sciencedirect.com/science/article/pii/S0927775713009102. http://dx.doi.org/10.1016/j.colsurfa.2013.11.045.

• of special interest.
•• of outstanding interest.